AIAA JOURNAL
Vol. 46, No. 1, January 2008

Static/Dynamic Buckling of Axially Compressed Thin-Walled Cylindrical Shells Using Simple Models

Anthony Kounadis*
Academy of Athens, 115 27 Athens, Greece

DOI: 10.2514/1.29861

The postbuckling response of elastic thin-walled circular cylindrical shells under axial compression is discussed using equivalent 1 and 2 degrees-of-freedom imperfect models characterized by a nonlinear spring component simulating the analogous restraining membrane force in the shell. The initial geometric shell imperfections are related to the out of straightness of shell generators. Very recently, Bodner and Rubin ("Modeling the Buckling of Axially Compressed Elastic Cylindrical Shells," *AIAA Journal*, Vol. 43, No. 1, 2005, pp. 103–110) proposed a 1 degree-of-freedom mechanical model, whose buckling mechanism can be viewed as a local event governed by a shallow archlike behavior depending on the shell geometry, which they related to an empirical formula based on experimentally measured shell buckling loads. This formula, relating the critical load to the ratio thickness-to-radius of the shell, was used for determining the aforementioned nonlinear spring component, necessary for the subsequent analysis of the model. In the present analysis, a new, more reliable 2 degree-of-freedom model for both axisymmetric and asymmetric buckling mechanisms of axially compressed circular cylindrical shells is proposed which can include antisymmetric imperfections and mode coupling. Another advantage of the proposed models is their ready extension to the dynamic buckling. Moreover, a semi-empirical formula is proposed which generalizes Koiter's formula to include the effect of the ratio thickness-to-the shell radius. Numerical examples illustrate the simplicity and efficiency of the analysis for establishing static and dynamic buckling estimates, quite satisfactory for structural design purposes.

Nomenclature

E	=	Young modulus of elasticity
E	=	total energy
F	=	dimensional (physical) spring force
F	=	dimensionless spring force, $=F/k\ell$
K	=	total kinetic energy
k	=	linear spring component
ℓ	=	length of the rigid link
m	=	concentrated mass
P	=	external dimensional (physical) load
P_c	=	dimensional bifurcational buckling load
P_s	=	dimensional limit point (peak) load
R	=	radius of the circular cylindrical shell
t	=	shell thickness
V	=	total potential energy
V_i	=	first derivative of V with respect to θ_i, $i = 1, 2$
V_{ij}	=	second derivative of V with respect to θ_i and θ_j, $i, j = 1, 2$
Δ	=	horizontal displacement
Δ	=	dimensionless horizontal displacement
δ, γ	=	quadratic and cubic nonlinear spring components, respectively
ε_i	=	initial angle imperfection, $i = 1, 2$
θ_0	=	initial angle imperfection, 1 degree-of-freedom model
θ	=	total angle (coordinate) defining the model deformed state
θ_i	=	total angle ($i = 1, 2$) defining the model deformed state
θ_D	=	total angle corresponding to dynamic buckling
κ	=	thickness-to-radius ratio, $=t/R$
κ_0	=	constant ratio t/R, $=0.0125$
λ	=	dimensionless load, $=P/P_c$
λ_c	=	dimensionless bifurcational load, $=1$
λ_s	=	dimensionless limit point (peak) load
λ_D	=	dimensionless dynamic buckling load
$\tilde{\lambda}_D$	=	lower bound dynamic buckling load
ν	=	Poisson's ratio
τ	=	time

Received 22 January 2007; revision received 29 August 2007; accepted for publication 2 September 2007.

*Professor-Academician, Soranou Efessiou 4.

I. Introduction

IN THE last decades, considerable attention has been paid to the effect of nonlinearities on the stability of structural systems. This is justified by the fact that application of a linear (bifurcational) analysis may fail to predict the actual (critical) buckling load. Indeed, this is true when the critical bifurcation point is unstable, implying a serious reduction of the load-carrying capacity due to unavoidable initial geometric imperfections. On the other hand, one should note that the majority of actual systems, if accurately modeled, exhibit a limit point instability rather than bifurcational buckling. This requires a complete nonlinear stability analysis for estimating the exact buckling load and the associated load-carrying capacity.

This study deals with the postbuckling analysis of thin-walled cylindrical shells under axial compression. Early studies on these shells have shown that their actual load-carrying capacity can be safely obtained via only a nonlinear analysis because classical (linear) analyses may lead to completely unacceptable results. On the other hand, extensive tests have shown that the theoretically predicted minimum postbuckling (peak) load is unrealistic to be useful as a guide for designers, particularly in case of very thin shells [1,2]. The discrepancy between test and theory rendered Koiter's [3] initial postbuckling analysis application necessary or other stability analyses combined with empirical formulas based on tests results. According to Koiter's theory, the limit point (peak) load for a circular cylindrical shell depends on the Poisson's ratio and mainly on small geometric imperfections, whose variety and measuring has been the subject of a lot of work for unstiffened and stiffened shells [1,2,4,5]. These shells are very sensitive to initial geometric imperfections, because the critical buckling load corresponds to a mode with axial and circumferential wavelength quite small compared to the shell radius.

Recently, Calladine [6] proposed an empirical formula for the limit point (peak) load based on the test results of Brush and Almroth [1]. A possible way of reconciling Koiter's load with the empirical Calladine's formula is to assume that geometric imperfections in Koiter's analysis depend also on the ratio (t/R) of thickness-to-radius of the shell. Brush and Almroth [1] have shown the dramatic discrepancy between test and theory over a wide range of the ratio t/R and the ratio L/R, where L is the shell length. The discrepancy increases with the decreasing ratio t/R (i.e., as the shell becomes thinner), which implies an extreme sensitivity of the buckling load due to initial imperfections. Experiments also show that for a given value of t/R, there is a considerable scatter in the buckling (collapse) loads. Hence, a reliable modeling of the shell buckling mechanism should include both effects, i.e., initial geometric imperfections and the ratio t/R.

Despite the existence of more than 2000 studies devoted to the buckling of axially compressed thin-walled circular cylindrical shells, the relative research continues in an attempt to improve existing treatments (see, e.g., Bushnell [2]). A main reason for this interest lies in the fact that the geometric imperfections have not as yet been fully identified. According to test observations by Singer et al. [7,8], it was deduced that the onset of buckling in these shells is highly localized over a small region. Thereafter, the buckling deformation assumes a diamond-shaped pattern, which is progressively repeated in neighboring sections, whereas the load drops suddenly at fixed overall shortening. It was also found that the membrane response due to such localized buckling is nonlinear and analogous of a nonlinear (soft) spring. Very recently, Bodner and Rubin [9], on the basis of testing on emptied beer cans, concluded that the buckling process is that of a local longitudinal strip supported at its middle by an elastic foundation which exhibits snap-through caused by the shallow archlike behavior in the circumferential direction. Bodner and Rubin presented an interesting reexamination of this problem by using a single mode mechanical model (similar to that of Budiansky and Hutchinson [10], Hutchinson and Budiansky [11], and Kounadis [12]) which experiences some of the salient buckling characteristics of uniformly axially compressed circular cylindrical shells.

In the present paper, being an extension of the last work by Bodner and Rubin [9] and Kounadis [13], two imperfection sensitive mechanical models [1 and 2 degrees of freedom (DOF)] consisting of rigid links are proposed for modeling the axisymmetric buckling of uniformly axially compressed circular cylindrical shells under static and dynamic (step) loading. The first one, much simpler than the single mode model of Bodner and Rubin [9], neglects the change of the bar link length without any practical effect on the accuracy of the obtained results [14]. The second mechanical 2-DOF model [15,16] is more reliable than 1-DOF models because it can include the coupling mode effect as well as symmetric or antisymmetric (out of straightness) imperfections. Note that the 2-DOF model with symmetric imperfections allows the analysis of both types of buckling mechanism of axially compressed circular cylindrical shells with axisymmetric imperfections; namely axisymmetric and asymmetric buckling. The latter type of asymmetric buckling occurs via an unstable symmetric bifurcation [16]. A further advantage of the proposed analysis is that it can be readily extended to the case of dynamic (step) load. Numerical examples illustrate the simplicity, efficiency, and reliability for structural design purposes of the approach proposed herein.

II. Mathematical Analysis

In this section, attention will be focused on the description of the basic equations governing the postbuckling response of the preceding axially compressed thin-walled circular cylindrical shells. The static and dynamic (due to a step load) response of these shells will be correlated to those of two mechanical (1-DOF and 2-DOF) spring models. Attention is focused on the choice of models to include the salient features of the shell axisymmetric buckling mechanism.

From early studies on axially compressed circular cylindrical shells, it is known [17] that 1) the buckling mechanism can be regarded as that of a longitudinal strip (i.e., shell generator) supported transversely by a "foundation" of elastic springs, and 2) the resulting shell extension in the circumferential direction is a nonlinear function of the transverse deflection. Hence, the supporting springs should be nonlinear elastic and also of soft type due to the imperfection sensitivity of these shells (implying a tremendous reduction of the collapse load). Moreover, it was found that experimentally obtained buckling loads were much lower than the theoretical ones. This is mainly attributable to initial geometric imperfections, among which the out of straightness of generators seems to be more important than that of circumferential out of roundness. Koiter's initial postbuckling analysis [3] was a very important contribution to the buckling of geometrically imperfect shells. However, the considerable "scatter" between tests and theory seems also to be attributed to the indeterminacy of the boundary conditions, the self-weight effect on the buckling [6], loading conditions, and friction effects. If these effects are a priori identified, one can establish a complete nonlinear analysis via numerical simulation for determining the critical buckling loads [18]. However, these effects are not known (e.g., the pattern variety and measuring of imperfections continue to be the subject of pertinent research). One way to overcome this difficulty is to adopt the so-called knockdown factor yielding a lower bound buckling estimate to all existing experimental results [19].

In view of the preceding information, one should seek readily employed approximate analyses leading to buckling estimates satisfactory for structural design purposes. Recently, Calladine [6], after statistical elaboration of almost 200 experimentally measured buckling loads, proposed the empirical formula

$$\sigma_{\text{mean}}/\text{E} = 5(t/R)^{1.5} \tag{1}$$

where σ_{mean} is the *mean* experimental buckling stress and E is the Young modulus of elasticity, R is the shell radius and t is its thickness. Practically, the test data points lie within two standard deviations related to upper and lower bounds corresponding to the mean stress multiplied by 2 and 0.5, respectively. Note that von Kármán et al. [17], on the basis of a small number of experiments, suggested a similar empirical formula but with an exponent 1.4 instead of 1.5. Recall that according to the classical (linearized) theory of buckling of cylindrical shells [20], the compressive buckling stress is

$$\sigma_c/\text{E} = 0.6(t/R) \tag{2}$$

Subsequently, σ_{mean} will be used as the limit point (peak) stress $\sigma_s(=\sigma_{\text{mean}})$. Thus, combining Eqs. (1) and (2), one can establish the empirical formula

$$\sigma_s/\sigma_c = 8.3\kappa^{1/2} \tag{3}$$

where $\kappa = t/R$.

For axially compressed cylindrical shells with axisymmetric imperfections, Koiter [3] has given the approximate formula

$$(1-\sigma_s/\sigma_c)^2 = [3\sqrt{3(1-\nu^2)}/2](\sigma_s/\sigma_c)\psi$$
$$\text{or} \quad (1-\sigma_s/\sigma_c)^2 = 2.478(\sigma_s/\sigma_c)\psi \tag{4}$$

where ψ is the geometric imperfection amplitude divided by the shell thickness. The empirical formula (3) can be related to the theoretical one in Eq. (4), if one assumes that ψ depends on the ratio [9] κ.

Singer et al. [7,8], on the basis of a lot of test observations, concluded that the onset of buckling of uniformly axially compressed circular cylindrical shells is highly localized over a small region. Subsequently, a diamond-shaped pattern is developed which can be viewed as that of a buckled longitudinal strip (i.e., shell generator) supported at each center by a nonlinear softening spring, implying an archlike behavior in the circumferential direction. Although the prebuckling deformation entails rotations, such rotations are very small or confined to a small region of the shell surface and thus the

influence of prebuckling nonlinearity can be neglected. The Brazier ovalization effect [2] referring to infinitely long shells is also neglected. On the basis of these observations (supplemented by tests on emptied beer cans) and the fact that these shells buckle abruptly and even explosively, Bodner and Rubin, in the aforementioned very interesting paper [9], proposed a 1-DOF mechanical model (used by Budiansky and Hutshinson [10,11] and Kounadis [12]) to simulate the axisymmetric buckling of imperfect axially compressed circular cylindrical shells. Because shell membrane response, as stated before, is nonlinear and the collapse (limit point) load drops suddenly after buckling, the model's spring should be nonlinear elastic of soft type. Bodner and Rubin's model [9] supported on an elastic cubic softening spring includes the effect of axis deformation in both bars. Moreover, in correlating the basic parameters of the model to those of the shells, they considered the nonlinear spring component as a function of the ratio κ characterizing the basic shell geometry. The other parameter which affects the buckling (limit point) load is the geometric imperfection which assumes the form of an initial angle, being more suitable than a displacement.

Subsequently, two mechanical imperfection-sensitive models of 1-DOF and 2-DOF, respectively, are proposed to simulate the axisymmetric buckling mechanism of geometrically imperfect circular cylindrical shells with symmetric and antisymmetric (for the 2-DOF model) imperfections under uniform axial compression. The models exhibit the salient features of the shells under discussion and mainly that of localized buckling of a longitudinal strip (shell generator) supported at its middle by a softening spring implying an archlike behavior. In both models, consisting of rigid links supported on nonlinear elastic softening springs, the effect of axial deformation of the links is neglected. As was shown [14,21], such effect on the limit point (peak) load, and particularly on the postbuckling path, is negligibly small for perfect models and even more for the imperfect models under consideration. The static stability analysis is readily extended to the case of dynamic buckling in both models.

III. Mechanical Model of 1-DOF

Consider the 1-DOF mechanical model of Fig. 1, consisting of two rigid links of equal length ℓ interconnected to each other through a frictionless hinge [12]. A concentrated mass m attached at the hinge is supported by a nonlinear elastic quadratic softening spring characterized by a linear and a nonlinear (dimensionless) component $k > 0$ and $\delta > 0$, respectively. An initial geometric imperfection is identified by an angle θ_0 measured from the straight (unstressed) configuration, whereas θ is the total angle due to the action of an axial (horizontal) end load P. Under the action of P, the following dimensionless spring force F is developed

$$\mathrm{F} = F/k\ell = (\sin\theta - \sin\theta_0)[1 - \delta(\sin\theta - \sin\theta_0)] \tag{5}$$

For compression the maximum of the curve F vs θ occurs when $\sin\theta = \sin\theta_0 + 1/2\delta$ and $\mathrm{F} = 1/4\delta$. In case of an elastic cubic softening spring with a nonlinear component γ, Eq. (5) becomes

$$\mathrm{F} = (\sin\theta - \sin\theta_0)[1 - \gamma(\sin\theta - \sin\theta_0)^2] \tag{5a}$$

whose maximum of F vs θ occurs when $\sin\theta = \sin\theta_0 + 1/\sqrt{3\gamma}$ and $\mathrm{F} = 2/3\sqrt{3\gamma}$.

A. Static Buckling Load

The total potential energy (TPE) function V of the model is given by

$$V = \frac{1}{2}(\sin\theta - \sin\theta_0)^2 - \frac{\delta}{3}(\sin\theta - \sin\theta_0)^3 - \lambda(\cos\theta_0 - \cos\theta) \tag{6}$$

where $\lambda = P/P_c$ and $P_c = k\ell/2$ is the bifurcational load of the perfect model (i.e., for $\theta_0 = 0$).

The equilibrium equation and the critical state are given by the derivatives $V_1 = \vartheta V/\vartheta\theta = 0$ and $V_{11} = \vartheta^2 V/\vartheta\theta^2 = 0$, respectively, i.e.,

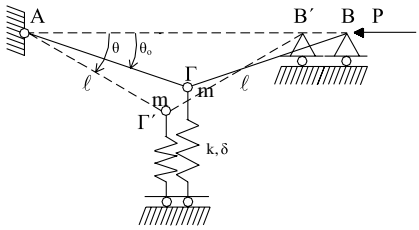

Fig. 1 Imperfect mechanical model of 1-DOF under end load *P*.

$$V_1 = (\sin\theta - \sin\theta_0)[1 - \delta(\sin\theta - \sin\theta_0)]\cos\theta - \lambda\sin\theta = 0 \tag{7}$$

$$V_{11} = [1 - 2\delta(\sin\theta - \sin\theta_0)]\cos^2\theta - [\sin\theta - \sin\theta_0 - \delta(\sin\theta - \sin\theta_0)^2]\sin\theta - \lambda\cos\theta = 0 \tag{8}$$

Clearly, the solution of Eqs. (7) and (8) for given δ yields the buckling (limit point) load λ_s and the corresponding angle θ_s.

Multiplying V_1 by $\sin\theta$ and V_{11} by $\cos\theta$, after adding the resulting equations, we obtain

$$\lambda = [1 - 2\delta(\sin\theta - \sin\theta_0)]\cos^3\theta \tag{9}$$

Following the procedure of Bodner and Rubin [9], we adopt the Calladine formula [6] for the buckling limit point (peak) load, $\lambda = \lambda_s$, according to which

$$\lambda_s = P_s/P_c = 8.3\kappa^{1/2} \tag{10}$$

where P_s is the limit point load and $\kappa = t/R$ is the ratio of the thickness-to-radius of the shell.

From Eqs. (9) and (10) one can determine δ for given values of θ_0 and κ via the relationship

$$\delta = \frac{\cos^3\theta - 8.3\kappa^{1/2}}{2(\sin\theta - \sin\theta_0)\cos^3\theta} \tag{11}$$

where apparently $\theta = \theta_s$ is the angle at the limit point.

Introducing the preceding expression of δ into Eq. (7) and using formula (10), we obtain

$$\cos^3\theta = 8.3\kappa^{1/2}\left(\frac{\sin\theta\cos 2\theta + \sin\theta_0}{\sin\theta - \sin\theta_0}\right) \tag{12}$$

From Eq. (12), one can determine for given values of κ and θ_0 the smallest value, $\theta = \theta_s$, corresponding to the peak (limit point) value in the nonlinear equilibrium path λ vs θ. Inserting $\theta = \theta_s$ into relation (11), we determine the nonlinear spring component δ and thereafter one can establish the nonlinear equilibrium path, λ vs θ, using Eq. (7).

One can also evaluate the horizontal displacement Δ of the loaded end via the relation

$$\Delta = \Delta/\ell = \cos\theta_0 - \cos\theta \quad \text{or} \quad \cos\theta = \cos\theta_0 - \Delta \tag{13}$$

Equation (13) for $0 < \theta < \pi/2$ yields

$$\sin\theta = [1 - (\cos\theta_0 - \Delta)^2]^{1/2} \tag{14}$$

Introducing the expressions of $\cos\theta$ and $\sin\theta$ from Eqs. (13) and (14) into the equilibrium Eq. (7), we can establish the corresponding path in terms of λ and Δ which allows us to compare it with that presented by Bodner and Rubin [9]. For the perfect model ($\theta_0 = 0$), Eq. (7) gives the equilibrium path λ vs Δ, through the following equation

$$\lambda = \{1 - \delta[1 - (1 - \Delta)^2]^{1/2}\}(1 - \Delta) \tag{15}$$

Figure 2 shows the equilibrium paths λ vs Δ of the perfect and imperfect model (with $\theta_0 = 1$ deg) corresponding to four cases: $\kappa = 0.01, 0.001, 0.003, 0.0003$. In all cases the static buckling load (SBL) corresponds to a limit point load λ_s.

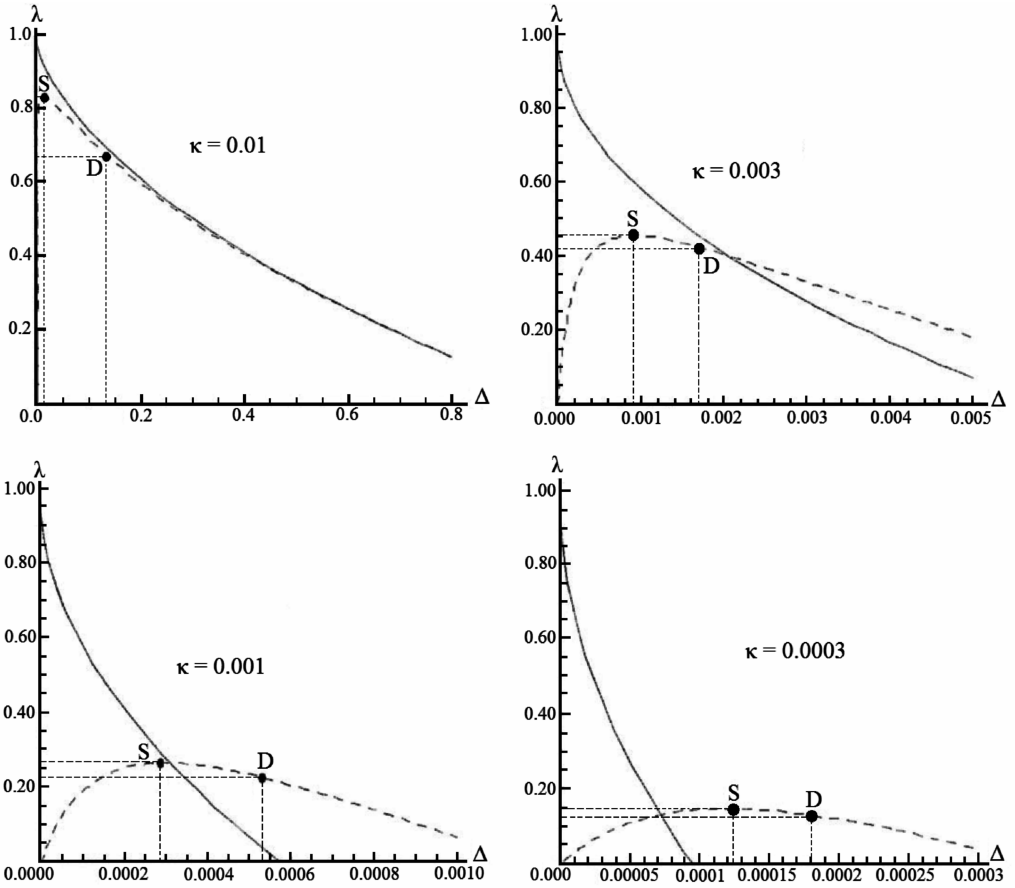

Fig. 2 Equilibrium paths λ vs Δ of the perfect (solid line) and imperfect (dashed line) model with $\theta_0 = 1$ deg in four cases: κ (=0.01, 0.001, 0.003, 0.0003).

Before comparing numerical results in graphical form of this work with those of Budner and Rubin [9], it is worth noticing the following:

If the preceding soft type quadratic model ($\delta > 0$) is perfect ($\theta_0 = 0$), it is related to an asymmetric bifurcation which is more sensitive to initial imperfections than the unstable symmetric bifurcation occurring by replacing the quadratic component δ by a cubic one $\gamma > 0$. The bifurcational load $\lambda_C = 1$ is independent of δ and γ, but the physical (dimensional) buckling load $P_c = k\ell/2$ depends on the linear spring component k.

From Fig. 3, we can compare the equilibrium paths λ vs Δ of this study with those presented by Bodner and Rubin [9] for an imperfect model with $\theta_0 = 1$ deg. It is clear that for $\kappa < 0.01$, the nonlinear equilibrium paths are more stiff in this analysis than those of Bodner and Rubin's paper. This is justified from the fact that the nonlinear spring component of this analysis is quadratic, whereas that of Bodner and Rubin is cubic.

Consequently, at each level of the loading, the former displacements are smaller than the latter ones. Note also, as observed by Bodner and Rubin [9], their model in case of $\theta_0 = 1.5$ deg shows that the dependence of the buckling loads on $\kappa = t/R$ is very similar to the NASA design curve [19]. The present study could also use a nonlinear spring component of cubic (softening) type. Regardless of this, the important conclusion that is drawn is that the results of the present very readily employed analysis which neglects the effect of axial deformation are quite satisfactory for structural design purposes. Thus, after the rather easy determination of the nonlinear spring component, one can establish the buckling and postbuckling path of the imperfect circular cylindrical shell through the corresponding simple analysis of the mechanical model. As shown next, the latter path is very important for establishing dynamic buckling loads (DBLs).

B. Dynamic Buckling Load

The preceding static analysis can be readily extended to the case of dynamic buckling due to a suddenly applied load of constant magnitude and infinite duration. Application of the principle of conservation of energy of the total potential (Hamiltonian) energy E between any two states gives [15,22]

$$E = K + V \tag{16}$$

where K is the (positive definite) total kinetic energy and V is the total potential energy, respectively, both of which are zero at $\tau = 0$ for this autonomous undamped system. Hence, $E = 0$ throughout the motion, which leads to

$$V = -K \tag{17}$$

Following Lagrange or Laplace dynamic (global) stability criterion dynamic buckling (in the large) for autonomous systems is defined as that state for which an escaped motion (through a saddle or its neighborhood with zero or nearly zero $V < 0$) becomes either unbounded or of very large (but bounded) amplitude [15]. The minimum load corresponding to this state is defined as the dynamic buckling load.

In case of autonomous undamped 1-DOF systems, dynamic buckling occurs always via a saddle with $V = 0$. Because such a point is an equilibrium point on the (static) unstable path, then $K = 0$, which, due to Eq. (16), because E (at time $\tau = 0$) $= 0$, yields [12,15,22]

$$V = 0 \tag{18}$$

Solution of Eq. (18), together with the equilibrium equation

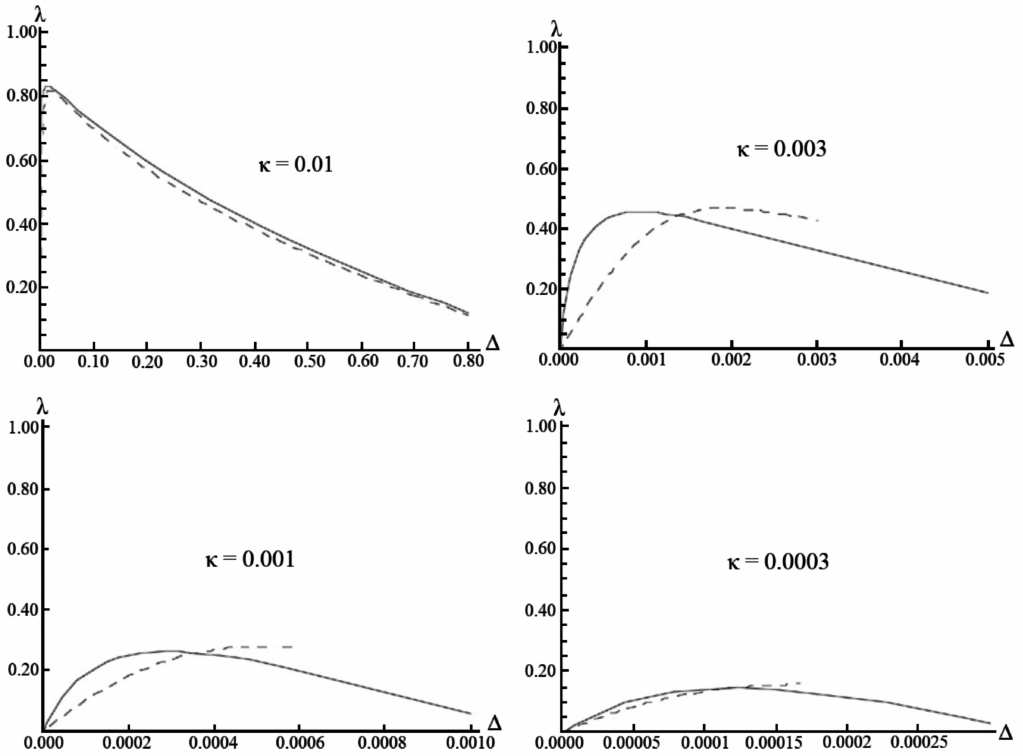

Fig. 3 Equilibrium paths based on this analysis (solid line) and Bodner and Rubin's work [9] (dashed line) for four cases of κ (=0.01, 0.001, 0.003, 0.0003).

$$V_1 = 0 \tag{19}$$

leads to exact dynamic buckling loads λ_D and corresponding limit point angles θ_D for 1-DOF systems.

For 2-DOF systems, a dynamic buckling criterion leading to "exact" DBLs was presented recently by Kounadis [15].

Following the aforementioned procedure for the dynamic buckling, one can establish for the autonomous undamped circular cylindrical shells under step load, or its equivalent 1-DOF mechanical model, the exact DBL λ_D via Eqs. (18) and (19), i.e.,

$$V = V_1 = 0 \tag{20}$$

where

$$\left.\begin{aligned} \mathrm{V} &= \tfrac{1}{2}(\sin\theta - \sin\theta_0)^2 - \tfrac{\delta}{3}(\sin\theta - \sin\theta_0)^3 - \lambda(\cos\theta_0 - \cos\theta) = 0 \\ \mathrm{V}_1 &= [\sin\theta - \sin\theta_0 - \delta(\sin\theta - \sin\theta_0)^2]\cos\theta - \lambda\sin\theta = 0 \end{aligned}\right\} \tag{21}$$

with δ obtained from Eq. (11) for given θ_0 and κ [yielding via Eq. (12) the limit point angle $\theta = \theta_s$].

Solving the system of Eqs. (21) with respect to θ and λ, we determine the critical dynamic buckling quantities $\lambda = \lambda_D$ and $\theta = \theta_D$. Recall that θ_D corresponds to a saddle point on the postbuckling equilibrium path. Figure 2 shows (in addition to four limit points S) four saddles D with respective DBLs λ_D corresponding to four different cases of the shell geometry parameter κ(=0.01, 0.001, 0.003, 0.0003). Clearly, as κ decreases, $\lambda_D \to \lambda_S$.

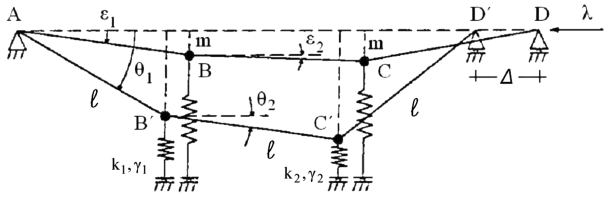

Fig. 4 Imperfect 2-DOF mechanical model under end load *P*.

IV. Mechanical Model of 2-DOF

Consider the 2-DOF model shown in Fig. 4 consisting of three weightless rigid links of equal length ℓ, hinged at each other, carrying two equal concentrated masses $m_1 = m_2 = m$. The masses are supported by two nonlinear elastic softening springs of cubic type with linear stiffness components $k_1 = k_2 = k > 0$ and nonlinear (dimensionless) ones $\gamma_1 = \gamma_2 = \gamma > 0$. The unrestrained configuration is defined by the initial geometric angle imperfections ε_1 and ε_2, and the deformed state by the angles θ_1 and θ_2 measured from horizontal lines. Because of the action of the horizontal load λ, the following spring forces, in dimensionless form, are developed, respectively,

$$\left.\begin{aligned} \mathrm{F}_1 &= F_1/k\ell = (\sin\theta_1 - \sin\varepsilon_1)[1 - \gamma(\sin\theta_1 - \sin\varepsilon_1)^2] \\ \mathrm{F}_2 &= F_2/k\ell = (\sin\theta_1 - \sin\varepsilon_1 + \sin\theta_2 - \sin\varepsilon_2)[1 - \gamma(\sin\theta_1 - \sin\varepsilon_1 + \sin\theta_2 - \sin\varepsilon_2)^2] \end{aligned}\right\} \tag{22}$$

Clearly, in case of an imperfect model with symmetric imperfections $\varepsilon_2 = 0$, and hence for symmetric buckling we also have $\theta_2 = 0$, which yields $F_2 = F_1$.

The total potential energy function V of a general imperfect system ($\varepsilon_2 \neq 0$) is given by [15]

$$\begin{aligned} V = {} & \frac{1}{2}(\sin\theta_1 - \sin\varepsilon_1)^2 - \frac{\gamma}{4}(\sin\theta_1 - \sin\varepsilon_1)^4 \\ & + \frac{1}{2}(\sin\theta_1 - \sin\varepsilon_1 + \sin\theta_2 - \sin\varepsilon_2)^2 \\ & - \frac{\gamma}{4}(\sin\theta_1 - \sin\varepsilon_1 + \sin\theta_2 - \sin\varepsilon_2)^4 \\ & - \lambda[\cos\varepsilon_1 + \cos\varepsilon_2 - \cos\theta_1 - \cos\theta_2 \\ & + \sqrt{1-(\sin\varepsilon_1 + \sin\varepsilon_2)^2} - \sqrt{1-(\sin\theta_1 + \sin\theta_2)^2}] \end{aligned} \tag{23}$$

where $\lambda = P/P_c$, with $P_c = k\ell/3$.

Given that $\pi/2 > \theta_i$ ($i = 1, 2$), the equilibrium equations resulting after differentiation of Eq. (23) with respect to θ_1 and θ_2 are

$$\begin{aligned} \frac{V_1}{\cos\theta_1} = {} & 2(\sin\theta_1 - \sin\varepsilon_1) - \gamma(\sin\theta_1 - \sin\varepsilon_1)^3 + \sin\theta_2 - \sin\varepsilon_2 \\ & - \gamma(\sin\theta_1 - \sin\varepsilon_1 + \sin\theta_2 - \sin\varepsilon_2)^3 \\ & - \lambda\left[\tan\theta_1 + \frac{\sin\theta_1 + \sin\theta_2}{\sqrt{1-(\sin\theta_1 + \sin\theta_2)^2}}\right] = 0 \end{aligned} \tag{24}$$

$$\begin{aligned} \frac{V_2}{\cos\theta_2} = {} & \sin\theta_1 - \sin\varepsilon_1 + \sin\theta_2 - \sin\varepsilon_2 \\ & - \gamma(\sin\theta_1 - \sin\varepsilon_1 + \sin\theta_2 - \sin\varepsilon_2)^3 \\ & - \lambda\left[\tan\theta_2 + \frac{\sin\theta_1 + \sin\theta_2}{\sqrt{1-(\sin\theta_1 + \sin\theta_2)^2}}\right] = 0 \end{aligned} \tag{25}$$

Subtracting Eq. (25) from Eq. (24), we obtain

$$\begin{aligned} & \sin\theta_1 - \sin\varepsilon_1 - \gamma(\sin\theta_1 - \sin\varepsilon_1)^3 - \lambda(\cot\theta_1 - \cot\theta_2) = 0 \\ & \text{or } \gamma = \frac{\sin\theta_1 - \sin\varepsilon_1 - \lambda(\tan\theta_1 - \tan\theta_2)}{(\sin\theta_1 - \sin\varepsilon_1)^3} \end{aligned} \tag{26}$$

Equations (24–26) can also be used for a quadratic spring constant δ if the cubic terms are replaced by quadratic ones. In either case, the critical (limit point) load is determined by vanishing the second variation of the TPE, $\delta^2 V = 0$, which leads to

$$\det[V_{ij}] = V_{11}V_{22} - V_{12}^2 = 0 (V_{12} = V_{21}) \tag{27}$$

where

$$\begin{aligned} V_{11} = {} & \{2 - 3\gamma(\sin\theta_1 - \sin\varepsilon_1)^2 \\ & - 3\gamma(\sin\theta_1 - \sin\varepsilon_1 + \sin\theta_2 - \sin\varepsilon_2)^2\}\cos^2\theta_1 \\ & - \{2(\sin\theta_1 - \sin\varepsilon_1) + \sin\theta_2 - \sin\varepsilon_2 - \gamma(\sin\theta_1 - \sin\varepsilon_1)^3 \\ & - \gamma(\sin\theta_1 - \sin\varepsilon_1 + \sin\theta_2 + \sin\varepsilon_2)^3\}\sin\theta_1 \\ & - \lambda\left\{\cos\theta_1 + \frac{\cos^2\theta_1 - (\sin\theta_1 + \sin\theta_2)[1-(\sin\theta_1 + \sin\theta_2)^2]\sin\theta_1}{[1-(\sin\theta_1 + \sin\theta_2)^2]^{3/2}}\right\} \\ V_{22} = {} & [1 - 3\gamma(\sin\theta_1 - \sin\varepsilon_1 + \sin\theta_2 - \sin\varepsilon_2)^2]\cos^2\theta_2 \\ & - [\sin\theta_1 - \sin\varepsilon_1 + \sin\theta_2 - \sin\varepsilon_2 \\ & - \gamma(\sin\theta_1 - \sin\varepsilon_1 + \sin\theta_2 - \sin\varepsilon_2)^3]\sin\theta_2 \\ & - \lambda\left\{\cos\theta_2 + \frac{\cos^2\theta_2 - (\sin\theta_1 + \sin\theta_2)[1-(\sin\theta_1 + \sin\theta_2)^2]\sin\theta_2}{[1-(\sin\theta_1 + \sin\theta_2)^2]^{3/2}}\right\} \\ V_{12} = {} & \left\{1 - 3\gamma\sin\theta_1 - \sin\varepsilon_1 + \sin\theta_2 - \sin\varepsilon_2)^2 \right. \\ & \left. - \frac{\lambda}{[1-(\sin\theta_1 + \sin\theta_2)^2]^{3/2}}\right\}\cos\theta_1\cos\theta_2 \end{aligned} \tag{28}$$

The nonlinear spring component γ (or δ) is determined via the preceding procedure by using the empirical Calladine formula (3) or Eq.(10), i.e.,

$$\lambda_s = P_s/P_c = 8.3\kappa^{1/2} (\kappa = t/R) \tag{29}$$

A. Static Buckling Load

Because λ_s, ε_1, and ε_2 are a priori known, after inserting into Eq. (25) the expression of γ from relation (26), one can establish the critical (limit point) angles θ_1^s and θ_2^s by solving the system of the nonlinear Eq. (24) [or Eq. (25)] and Eq. (27). Thereafter, inserting the values of θ_1^s and θ_2^s into Eq. (26), we obtain the value of γ.

Subsequently, inserting this value of γ into Eqs. (24) and (25), we can establish the nonlinear equilibrium paths $\lambda = \lambda(\theta_1, \theta_2)$ for various levels of the external load λ for a symmetric model with symmetric imperfections, $\varepsilon_2 = 0$ (Fig. 5). Note that asymmetric buckling occurs before the limit point (related to symmetric buckling) through an unstable symmetric bifurcation lying on the nonlinear prebuckling path. The nonlinear equilibrium path of the perfect system is obtained in an asymptotic sense by using a very small value of ε_1 (i.e., $\varepsilon_1 = 10^{-6}$).

Figure 6 shows four nonlinear equilibrium paths λ vs Δ, corresponding to $\varepsilon_1 = 1$ deg and four values of $\kappa(=0.01, 0.001, 0.003, 0.0003)$, where

$$\begin{aligned} \Delta = {} & [\cos\varepsilon_1 + \cos\varepsilon_2 - \cos\theta_1 - \cos\theta_2 \\ & + \sqrt{1-(\sin\varepsilon_1 + \sin\varepsilon_2)^2} - \sqrt{1-(\sin\theta_1 + \sin\theta_2)^2}] \end{aligned} \tag{30}$$

.

Note that for the rather thick shell with $\kappa = 0.01$, there is no bifurcation on the nonlinear equilibrium path and the 2-DOF model loses its stability via a limit point. For the sake of comparison, we have also included the corresponding equilibrium paths λ vs Δ of the previous 1-DOF quadratic model which for all κ are less stiff than those of the 2-DOF model. Figure 7 shows the value of the spring force F_1 corresponding to the buckling load of the four cases shown in Fig. 6. Note that in all cases F_1 is much less than its maximum (peak) value.

B. Dynamic Buckling Load

The preceding static analyses can be extended to the case of dynamic loading due to a suddenly applied load P of constant magnitude and infinite duration (autonomous system). The general procedure for a 2-DOF autonomous nondissipative system was comprehensively presented by the author [15]. The specific (quite simple) procedure for an imperfect 2-DOF system with symmetric imperfections was fully discussed very recently by Kounadis and Raftoyiannis [16]. According to this analysis, dynamic buckling

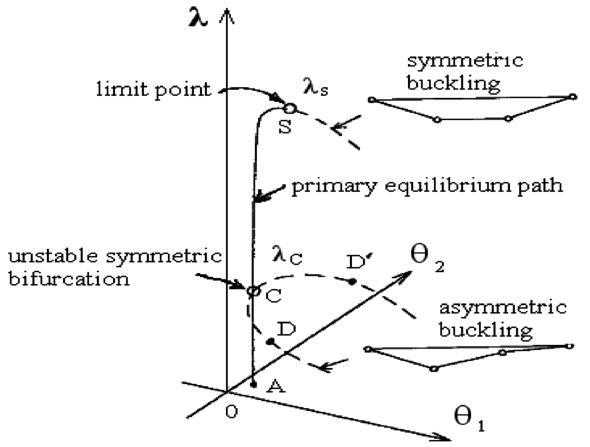

Fig. 5 Nonlinear equilibrium path $\lambda = \lambda(\theta_1, \theta_2)$ for a 2-DOF symmetric model with symmetric imperfections [16].

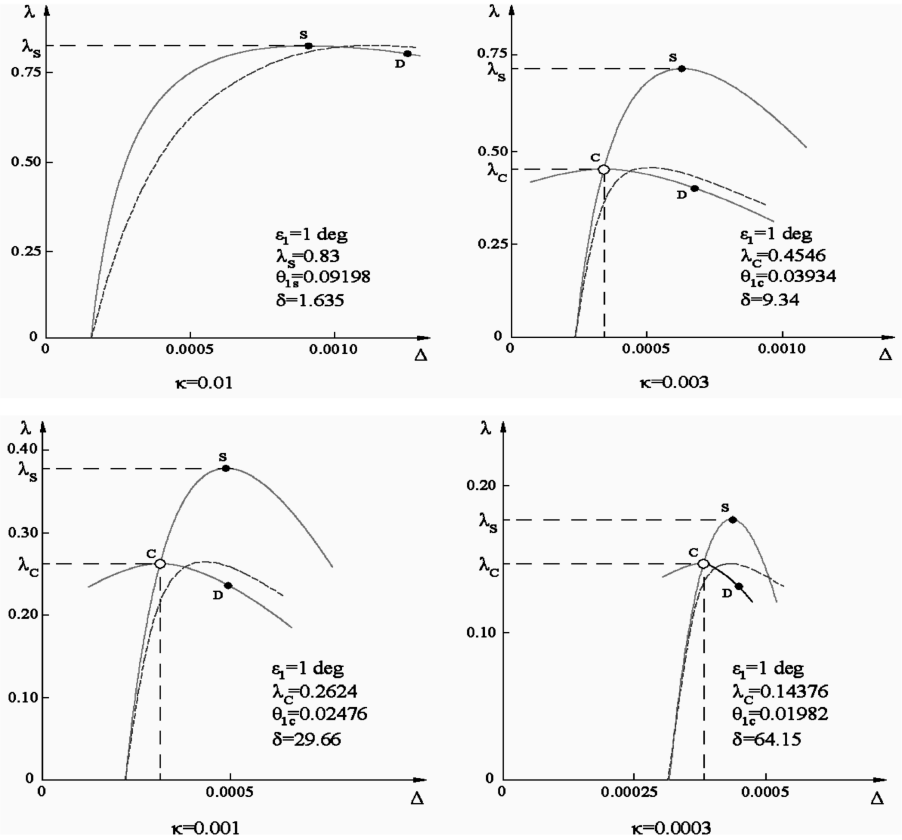

Fig. 6 Equilibrium paths λ vs Δ for two models (2-DOF, solid line and 1 DOF, dashed line) with $\varepsilon_1 = 1$ deg and four values of κ (=0.01, 0.001, 0.003, 0.0003).

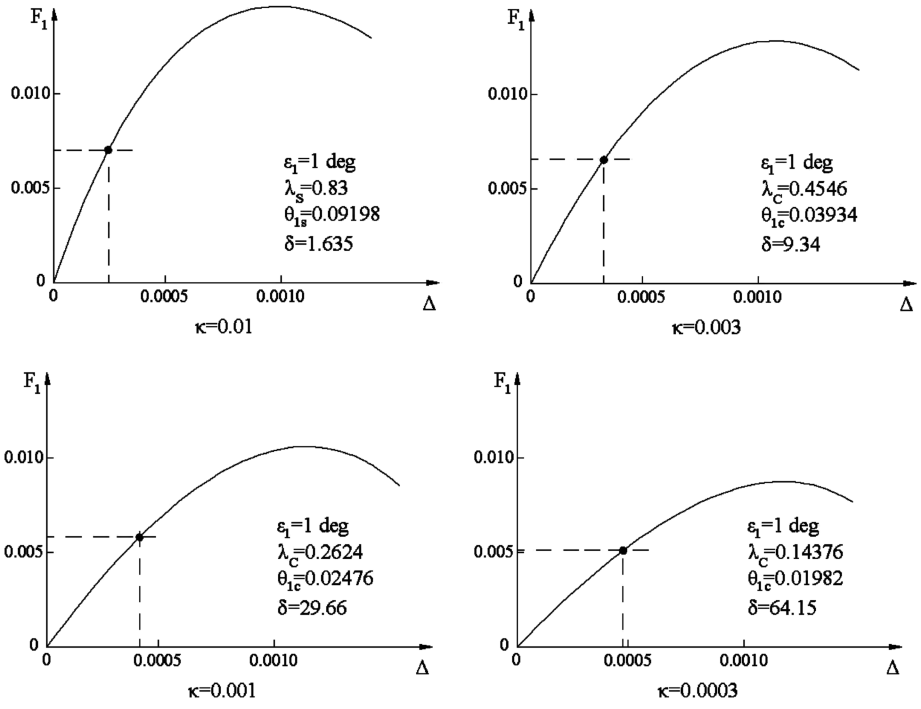

Fig. 7 Values of the spring force F_1 corresponding to the critical buckling loads related to the four previous cases of κ (=0.01, 0.001, 0.003, 0.0003) shown in Fig. 6.

(related to an escaped motion) occurs via the vicinity of either one of the two saddles D and D' lying on the unstable symmetric postbuckling path (Fig. 5), bifurcating from the nonlinear primary path. From Fig. 6, one can see the saddles D on the postbuckling path of the 2-DOF model. The DBL λ_D is obtained by using a geometric approach based on certain salient features of the zero-level TPE closed curve $V = 0$ in conjunction with the total energy-balance equation [14]. The first step is to determine a lower bound dynamic buckling estimate $\tilde{\lambda}_D$ by solving the system of Eqs. (24) and (25) (i.e., $V_1 = V_2 = 0$) together with $V = 0$. Figure 8a shows the closed curve

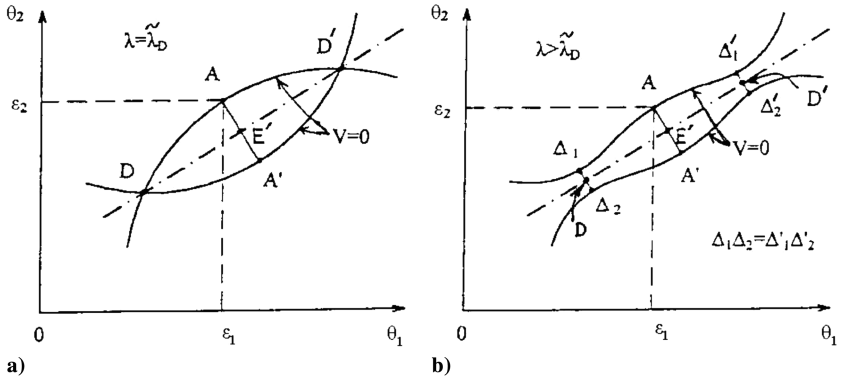

Fig. 8 The curve $V = 0$ in the plane $0\theta_1, \theta_2$: a) for $\lambda = \tilde{\lambda}_D$ (closed curve) and b) for $\lambda > \tilde{\lambda}_D$ (two symmetrical curves).

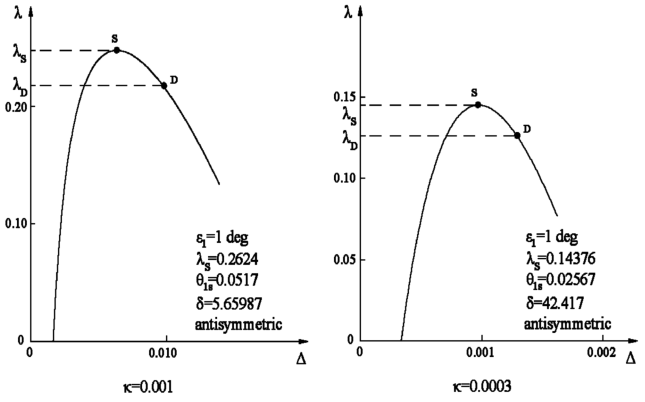

Fig. 9 Equilibrium paths λ vs Δ for α 2-DOF imperfect model with antisymmetric imperfections ($\varepsilon_1 = 1$ deg, $\varepsilon_2 = -2\varepsilon_1$) corresponding to $\kappa = 0.001$ and $\kappa = 0.0003$.

$V(\theta_1, \theta_2, \tilde{\lambda}_D) = 0$ passing through the two saddles D and D'. Subsequently, by step increasing the loading $\lambda(>\tilde{\lambda}_D)$, the corresponding TPE curve $V = 0$ is transformed into two symmetrical curves with equal distances at the saddles $\Delta_1\Delta_2 \equiv \Delta'_1\Delta'_2$ (Fig. 8b). When $\Delta_1\Delta_2 \equiv \Delta'_1\Delta'_2$ become equal to the distance of these curves at their axis of symmetry AA' (where A is the starting point of motion), then an escaped motion occurs (dynamic buckling). Such a state corresponds to the exact dynamic buckling load $\lambda_D(>\lambda_D)$ [16].

Finally, one could also consider the case of axially compressed cylindrical shells under antisymmetric initial imperfections. Then, the previous governing equations of the 2-DOF model shown in Fig. 4 are also valid with initial angle imperfection $\varepsilon_2 = -\sin^{-1}(2\sin\varepsilon_1) \cong -2\varepsilon_1$. The model under static loading loses always its stability via a limit point. Figure 9 shows the equilibrium paths λ vs Δ with the SBLs for an imperfect 2-DOF model with initially antisymmetric imperfections ($\varepsilon_1 = 1$ deg and $\varepsilon_2 = -2$ deg) corresponding to $\kappa = 0.001$ and 0.0003. The respective DBLs are also presented in Fig. 9. The cases $\kappa = 0.01$ and $\kappa = 0.003$, in which the nonlinear spring component should be of hard type, have been omitted.

V. Generalization of Koiter's formula

In this section, an attempt is made to reconcile Koiter's Eq. (4) with the empirical formula (3). This will be based on the following observations:

1) Koiter's analysis focuses attention on the initial postbuckling response, being exact in an asymptotic sense. This means that Koiter's analysis is exact at the bifurcation point itself and a close approximation for postbuckling patterns near the bifurcation point.

2) As observed by Bushnell [2], the most significant trend of Brush and Almroth [1] experimental data is the increasing discrepancy between theory and test with increasing R/t, namely when the shells become thinner. This trend indicates that the discrepancy arises from the extreme sensitivity of the critical load in very thin shells. In view of Koiter's formula (4) in terms of the loading ratio λ_s/λ_c, i.e.,

$$(1 - \lambda_s/\lambda_c)^2 = 2478(\lambda_s/\lambda_c)\psi \tag{31}$$

Eq. (31) can be considered reliable only in the vicinity of the critical load 1, say, e.g., for $0.90 < \lambda_s/\lambda_c \leq 1$. Hence, if the imperfection parameter ψ could also include the effect of the ratio $\kappa = t/R$, we should consider only very thick shells. For instance, for $\kappa = 0.0125$, the empirical formula (3) gives $\lambda_s/\lambda_c = 0.93$. Because, according to Koiter's analysis, ψ depends only on the initial geometric imperfections, one can write

$$(1 - \lambda_s/\lambda_c)^2 = 2.478(\lambda_s/\lambda_c)\theta_0 \tag{32}$$

Equation (32) for $\theta_0 = 0.5$ deg $= \pi/360$ yields $\lambda_s/\lambda_c = 0.93$, whereas for $\theta_0 = 1$ deg $= \pi/180$ gives $\lambda_s/\lambda_c = 0.90$.

On the basis of these observations, one should seek a semi-empirical formula for the critical load which could include both parameters (i.e., geometric imperfections and the ratio $\kappa = t/R$). Thus, the following extension of Koiter's formula is suggested

$$(1 - \lambda_s/\lambda_c)^2 = 2.48(\lambda_s/\lambda_c)\theta_0(\kappa_0/\kappa)^{2.8} \tag{33}$$

where $\kappa_0 = 0.0125$. This semi-empirical formula was derived after trials as an approximate average between existing theoretical and experimental results.

A comparison of the critical loads λ_s/λ_c based on formula (3), on Bodner–Rubin analysis [9], and the present approach [Eq. (33)], respectively, is given in Table 1 for two values of θ_0 (=1, 2 deg) and five values of κ_0/κ (1, 1.25, 4.167, 12.5, 41.67).

Note that the greater deviations in λ_s/λ_c between Eqs. (3) and (33), as well as between the Bodner–Rubin analysis [9] and the present one [Eq. (33)], occur in the thinner shells in which the uncertainty in determining critical loads is greater. Critical loads for $\kappa < 0.002$ are questionable. One should also clarify that other empirical formulas (possibly better) could be proposed. Note also that the results of Bodner–Rubin are slightly more conservative than the present results for $\kappa = 0.003$ and $\theta_0 = 1$ deg.

The proposed analysis could be supplemented by establishing a "knockdown" reduction factor which would be useful for structural design purposes. This can be achieved, e.g., by seeking an analogous formula to that given in Eq. (3). However, such a load reduction factor should be, in addition to the ratio t/R, a function of other parameters [2], such as fabrication and size of shells, and moreover of the length of shell in case of short shells for which the available number of tests is not sufficient.

Before closing this section, one should remark that a probabilistic approach in view of the randomness of initial imperfections of the shells under discussion (amplitude and/or shape in the axial and circumferential direction) could also be used, provided that large numbers of experimental data are available. However, such an approach, e.g., the powerful method of Monte Carlo, should also be combined with a deterministic analysis which is the cornerstone of

Table 1 Critical loads λ_s/λ_c based on Eq. (3), Bodner–Rubin analysis [9], and Eq. (33) for various values of θ_0 and κ

	Equation (3) λ_s/λ_c	κ_0/κ	Bodner–Rubin λ_s/λ_c		Equation (33) λ_s/λ_c	
$\kappa_0 = 0.0125$	0.93	1	$\theta_0 = 1$ deg	0.8844	$\theta_0 = 1$ deg	0.90
			$\theta_0 = 2$ deg	0.8346	$\theta_0 = 2$ deg	0.86
$\kappa = 0.01$	0.83	1.25	$\theta_0 = 1$ deg	0.8190	$\theta_0 = 1$ deg	0.84
			$\theta_0 = 2$ deg	0.7905	$\theta_0 = 2$ deg	0.82
$\kappa = 0.003$	0.45	4.167	$\theta_0 = 1$ deg	0.4672	$\theta_0 = 1$ deg	0.49
			$\theta_0 = 2$ deg	0.4567	$\theta_0 = 2$ deg	0.39
$\kappa = 0.001$	0.26	12.5	$\theta_0 = 1$ deg	0.2795	$\theta_0 = 1$ deg	0.14
			$\theta_0 = 2$ deg	0.2791	$\theta_0 = 2$ deg	0.10
$\kappa = 0.0003$	0.14	41.67	$\theta_0 = 1$ deg	0.1586	$\theta_0 = 1$ deg	0.03
			$\theta_0 = 2$ deg	0.1585	$\theta_0 = 2$ deg	0.02

every probabilistic approach. An interesting treatment on this subject is recently reported by Elishakoff et al. [23].

VI. Conclusions

In view of the various uncertainties (e.g., geometric imperfection, boundary and loading conditions, self-weight, etc.) affecting decisively the buckling mechanism of the shells under discussion, one has to resort to approximate analyses by combining theory with empirical formulas based on test data. Experiments have revealed the considerable effect of the ratio $\kappa = t/R$ on the reduction of the buckling loads, which, according to Koiter's theory, such a reduction is attributed only to initial geometric imperfections. The approximate analyses refer to the modeling of the buckling mechanism of the shells. Simple mechanical spring models of 1-DOF and 2-DOF are proposed for simulating the nonlinear buckling mechanism of imperfection-sensitive axially compressed circular cylindrical shells under static and dynamic loading. The major step is the choice of suitable spring models which should exhibit the salient buckling features of the shells under discussion (among which, a limit point instability for 1-DOF models, whereas for 2-DOF models with symmetric imperfections, either an unstable symmetric bifurcation or an asymmetric bifurcation). The nonlinear softening spring components affect appreciably the shape of the postbuckling path which becomes more sharp in the case of a quadratic spring than a cubic spring. Thus, the quadratic model is more sensitive to imperfections than the cubic one. The nonlinear spring component of the mechanical models is correlated to the shell geometry ($\kappa = t/R$) via an empirical formula based on statistical elaboration of experimental results.

The following constitute the most important concluding remarks and new findings:

1) The derivation of the governing equations of both models is based on their total potential energy function and its derivatives of first order (equilibrium equations) and second order (critical state). The proposed 2-DOF model, which includes the mode coupling effect, is more reliable than 1-DOF models used up until now. Indeed, the 2-DOF model can simulate both types of buckling mechanism of axially compressed thin-walled circular cylindrical shells with axisymmetric imperfections, i.e., axisymmetric (occurring via a limit point) and asymmetric buckling (occurring via an unstable symmetric bifurcation). Both models experience a nonlinear prebuckling equilibrium path with unstable postbuckling paths which become more abrupt in the presence of nonlinear softening springs. Between the two softening springs, the effect on the buckling load of the quadratic spring is more severe in the case of initial imperfections than that of the cubic spring.

2) The results of the present readily employed analysis (which neglects the effect of link axis deformation as negligibly small) are quite satisfactory for structural design purposes.

3) The bifurcational buckling load is independent of the nonlinear spring components δ and γ, whereas the physical (dimensional) buckling load depends on the linear spring component k.

4) As was presented in graphical form, the effect of both symmetric and antisymmetric initial geometric imperfections on the buckling and postbuckling response leads practically to the same results.

5) A semi-empirical formula is proposed which generalizes the well-known Koiter's formula by including the effect of the ratio thickness-to-shell radius. This was derived after trials as an approximate average between various existing theoretical and experimental results.

6) The present analysis gives also easily obtained dynamic buckling estimates, very satisfactory for structural design purposes. The dynamic buckling load is exact for 1-DOF models occurring via a saddle on the postbuckling path with $V = 0$, and for 2-DOF models, the DBL obtained through this analysis is practically exact occurring in the vicinity of a saddle on the postbuckling path with nearly zero $V(<0)$.

7) The imperfection sensitivity is more severe under dynamic loading than under static loading, which always is related to higher buckling loads (with smaller limit point displacements) than the dynamic ones (associated with greater dynamic displacements). This lies in the fact that the dynamic critical point is located on the postbuckling path beyond the limit point or the unstable bifurcation. However, as the ratio $\kappa = t/R$ decreases, the difference between these two buckling loads also decreases. For very thin shells, these loads are practically the same.

References

[1] Brush, D. O., and Almroth, B. O., *Buckling of Bars, Plates, and Shells*, McGraw–Hill, New York, 1975.

[2] Bushnell, D., *Computerized Buckling Analysis of Shells*, Martinus–Nijhoff, Dordrecht, The Netherlands, 1985.

[3] Koiter, W. T., "On the Stability of Elastic Equilibrium," (in Dutch), Ph.D. Thesis, Technological Univ. of Delft, Holland, The Netherlands, 1945; also NASA TT F-10 (in English), p. 833, 1967.

[4] Chrysanthopoulos, M. K., Baker, M. J., and Dowling, P. J., "Statistical Analysis of Imperfection in Stiffened Cylinders," *Journal of Structural Engineering*, Vol. 117, No. 7, 1991, pp. 1979–1998.

[5] Chrysanthopoulos, M. K., Baker, M. J., and Dowling, P. J., "Imperfection Modeling for Buckling Analysis of Stiffened Cylinders," *Journal of Structural Engineering*, Vol. 117, No. 7, 1991, pp. 1998–2017.

[6] Calladine, C. R., "A Shell-Buckling Paradox Resolved," *Advances in the Mechanics of Plates and Shells*, edited by D. Durban, D. Givoliand, and J. G. Simonds, Kluwer Academic, Norwell, MA, 2001, pp. 119–134.

[7] Singer, J., Arbocz, J., and Weller, T., *Buckling Experiments: Experimental Methods in Buckling of Thin-Walled Structures*, Vol. 1, Wiley, New York, 1998.

[8] Singer, J., Arbocz, J., and Weller, T., *Buckling Experiments: Experimental Methods in Buckling of Thin-Walled Structures*, Vol. 2, Wiley, New York, 2002.

[9] Bodner, S. R., and Rubin, M. B., "Modeling the Buckling of Axially Compressed Elastic Cylindrical Shells," *AIAA Journal*, Vol. 43, No. 1, 2005, pp. 103–110.

[10] Budiansky, B., and Hutchinson, J. W., "Dynamic Buckling of Imperfection-Sensitive Structures," *Proceedings of the 11th International Congress of Applied Mechanics*, Springer–Verlag, Berlin, 1966, pp. 636–651.

[11] Hutchinson, J. W., and Budiansky, B., "Dynamic Buckling Estimates," *AIAA Journal*, Vol. 4, March 1966, pp. 525–530.

[12] Kounadis, A. N., "Dynamic Stability Criteria of Non-Linear Elastic Damped/Undamped Systems Under Step Loading," *AIAA Journal*, Vol. 28, No. 7, 1990, pp. 1217–1223.

[13] Kounadis, A. N., "Recent Advances on Postbuckling Analyses of Thin-Walled Structures: Beams, Frames and Cylindrical Shells," *Journal of Constructional Steel Research: JCSR*, Vol. 62, 2006, pp. 1101–1115. doi:10.1016/j.jcsr.2006.06.014

[14] Kounadis, A. N., "Material-Dependent Stability Conditions in the Buckling of Nonlinear Elastic Bars," *Acta Mechanica*, Vol. 67, 1987, pp. 209–228. doi:10.1007/BF01182133

[15] Kounadis, A. N., "A Geometric Approach for Establishing Dynamic Buckling Loads of Autonomous Potential Two-Degree-of-Freedom Systems," *Journal of Applied Mechanics*, Vol. 66, March 1999, pp. 55–61.

[16] Kounadis, A. N., and Raftoyiannis, J., "Dynamic Buckling of a 2-DOF Imperfect System with Symmetric Imperfections," *International Journal of Non-Linear Mechanics*, Vol. 40, 2005, pp. 1229–1237. doi:10.1016/j.ijnonlinmec.2005.02.005

[17] Von Kármán, T., Dunn, L. G., and Tsien, H., "The Influence of Curvature on the Buckling Characteristics of Structures," *Journal of the Aeronautical Sciences*, Vol. 7, 1940, pp. 276–289.

[18] Arbocz, J., and Starnes, J. E., "On a High-Fidelity Hierarchical Approach to Buckling Load Calculations," *Solid Mechanics and Its Applications*, edited by H. R. Rew and S. Pellegrino, Vol. 104, Kluwer Academic, Norwell, MA, 2002, pp. 271–292.

[19] Timoshenko, S. P., and Gere, J. M., *Theory of Elastic Stability*, McGraw–Hill, New York, 1961, Sec. 11.1.

[20] Kounadis, A. N., and Mallis, J. G., "Two Efficient Approaches of Elastica Problem of Nonlinear Elastic Bars," *Journal of the Engineering Mechanics Division, ASCE*, Vol. 113, No. 5, 1987, pp. 766–779.

[21] Weingarten, V. I., Morgan, E. J., and Seide, P., "Elastic Stability of Thin-Walled Cylindrical and Conical Shells Under Axial Compression," *AIAA Journal*, Vol. 3, No. 3, 1965, pp. 500–505.

[22] Simitses, G. J., *Dynamic Stability of Suddenly Loaded Structures*, Springer–Verlag, New York, 1990.

[23] Elishakoff, I., Li, Y., and Starnes, G. H., *Non-Classical Problems in the Theory of Elastic Stability*, Cambridge Univ. Press, Cambridge, England, U.K., 2001.

K. Shivakumar
Associate Editor